Supplementary for

The impact of traffic on air quality in Ireland: insights from the simultaneous sampling of submicron aerosol at the kerbside and residential site

Chunshui Lin[1,2,3], Darius Ceburnis[1], Wei Xu[1,2], Eimear Heffernan[4], Stig Hellebust[4], John Gallagher[5], Ru-Jin Huang[1,2,3*], Colin O'Dowd[1*], and Jurgita Ovadnevaite[1]

[1]School of Physics, Ryan Institute's Centre for Climate and Air Pollution Studies, National University of Ireland Galway. University Road, Galway. H91 CF50, Ireland
[2]State Key Laboratory of Loess and Quaternary Geology and Key Laboratory of Aerosol Chemistry and Physics, Chinese Academy of Sciences, 710061, Xi'an, China
[3]Center for Excellence in Quaternary Science and Global Change, Institute of Earth Environment, Chinese Academy of Sciences, Xi'an 710061, China
[4]School of Chemistry and Environmental Research Institute, University College Cork, Cork, Ireland
[5]Department of Civil, Structural & Environmental Engineering, Trinity College Dublin, the University of Dublin, Ireland.

Correspondence to: Ru-Jin Huang (rujin.huang@ieecas.cn) and Colin O'Dowd (colin.odowd@nuigalway.ie)

Supplementary section of the chemical composition of PM_1, meteorological parameters, and gases (NO_x and CO)

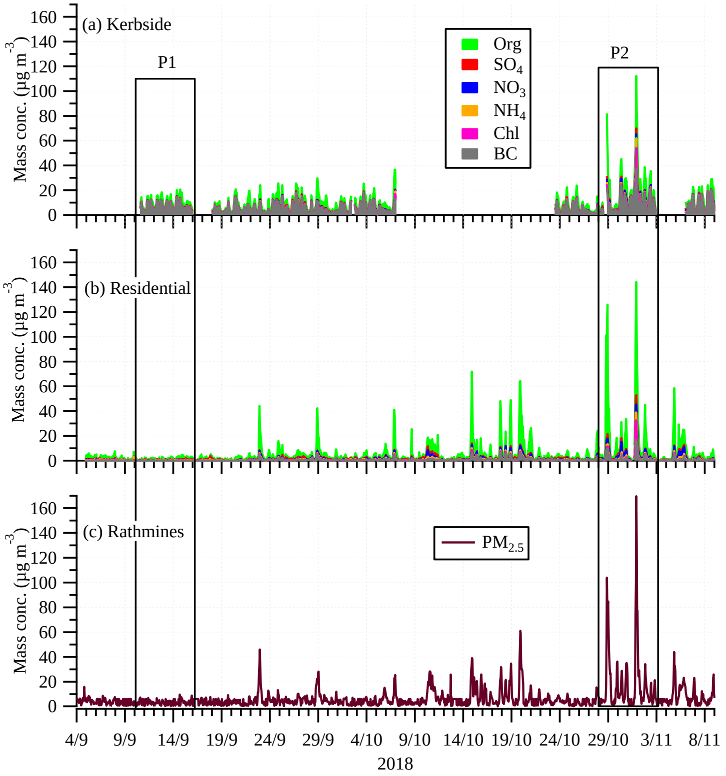

Figure S1. Time series of submicron organic aerosol (OA), sulfate (SO_4), nitrate (NO_3), ammonium (NH_4), chloride (Chl), and black carbon (BC) at the kerbside (top panel), residential site (mid panel), and EPA Rathmines station from 4 September to 9 November 2018. P1, from 10 September to 17 September, was selected to represent non-heating periods while P2, from 27 October to 4 November 2018, was selected to represent the heating period. Note that the ACSM and BC data were hourly averaged while the time resolution of $PM_{2.5}$ measurement was 1 h. The gaps at the measurement was due to ACSM malfunction at TCD.

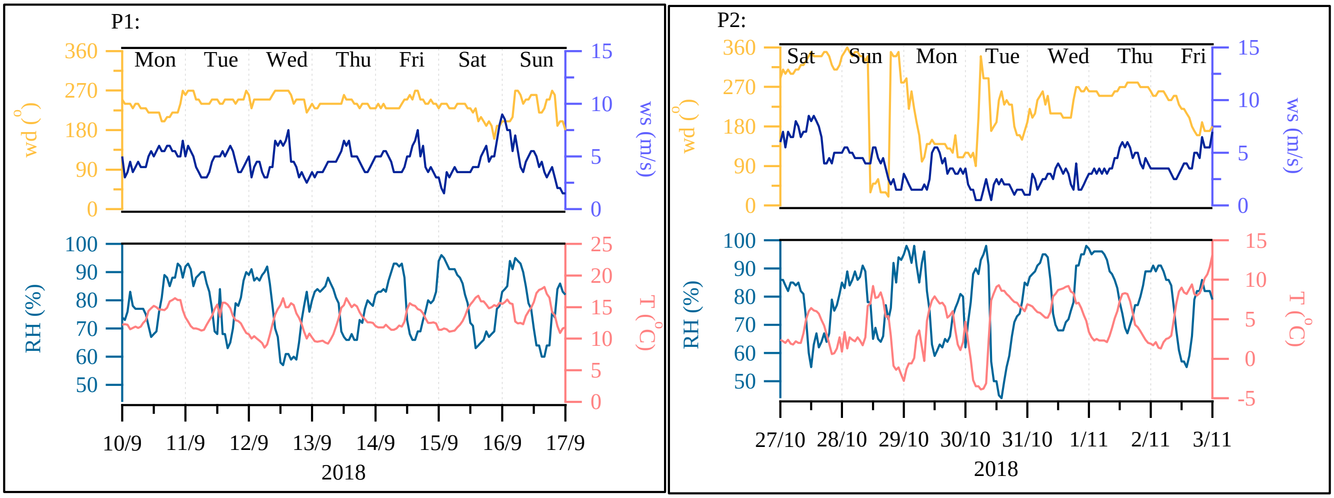

Figure S2. Time series of wind direction (wd), wind speed (ws), relative humidity (RH), and temperature (T) during P1 (left panel) and P2 (right panel).

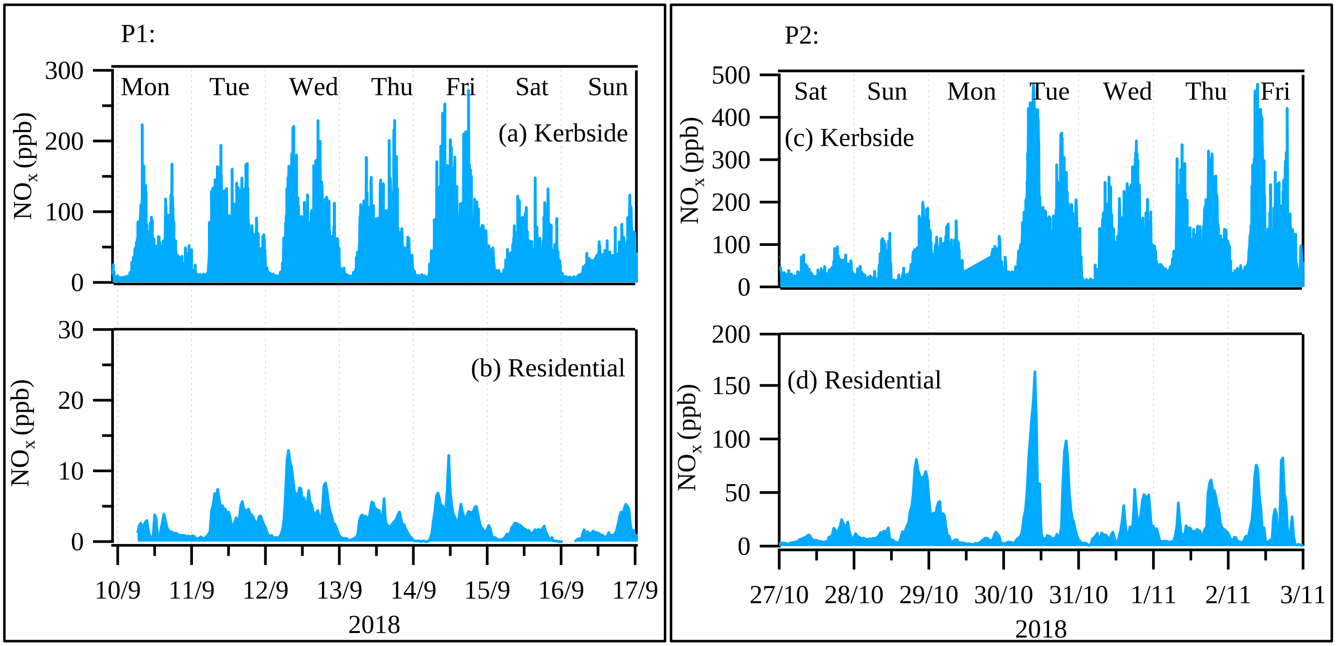

Figure S3. Time series of the mixing ratio of NO_x (ppbv) during P1 and P2 at the kerbside (a, c) and residential site (b, d). Also shown are the day of the week, including Monday (Mon), Tuesday (Tue), Wednesday (Wed), Thursday (Thu), Friday (Fri), Saturday (Sat), and Sunday (Sun).

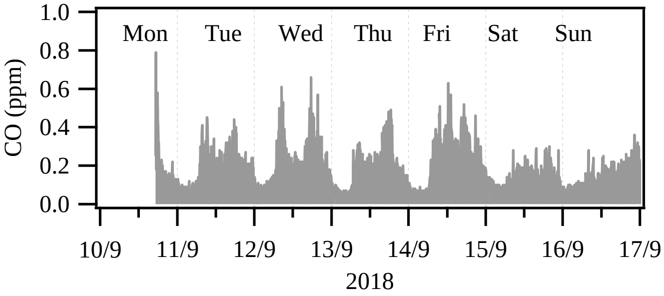

Figure S4. Time series of the mixing ratio of CO (ppmv) at the kerbside during P1. Note that the CO measurement was not available at the residential site. Also shown are the day of the week, including Monday (Mon), Tuesday (Tue), Wednesday (Wed), Thursday (Thu), Friday (Fri), Saturday (Sat), and Sunday (Sun).

Supplementary section of OA source apportionment

OA factors at the kerbside during P1.

To resolve the OA sources, unconstrained PMF (or free PMF) was firstly conducted on the OA matrix with a range of solutions from three to five factors. The solution that best represented the data was the three-factor solution because the solutions with more factors provided no meaningful but splitting from the already resolved factors (Fig. S5). The three-factor solution contained a hydrocarbon-like OA (HOA) factor from traffic, cooking-like OA (COA) factor from cooking sources, and an oxygenated OA (OOA) factor corresponding to the secondary processes.

Although the three-factor solution from free PMF could reasonably represent the data, there was still a certain extent of mixing between the factors because the cooking-like OA (COA) factor contained no signal at *m/z* 44 and a very low signal at 43 (Fig. S8) which was not physically meaningful (Mohr et al., 2012). To reduce the mixing between factors, the *a* value approach within ME-2 (Canonaco et al., 2013) was utilized by constraining the reference profile of HOA and COA (Crippa et al., 2013). A tight constraint or a small *a* value (i.e., 0.1) was applied for HOA because HOA was not expected to vary too much as indicated by the small variation of HOA profiles obtained from different sites across the world (Ng et al., 2011a). In contrast, COA could vary to some extent due to different styles of cooking and different types of food cooked (He et al., 2010; Mohr et al., 2012). To explore the solution space, an *a* value of 0-0.5 with a step of 0.1 was used to constrain the reference COA profile while keeping the *a* value of 0.1 constant for the HOA reference profile. The ME-2 results showed that the relative contributions of HOA (26% - 29%), COA (35% - 39%), and OOA (36% - 37%) to the total OA varied only by a few percents within the considered *a* values (Fig. S9), indicating the magnitudes (i.e., the *a* value of 0-0.5) of constraints on COA had a relatively small effects on the apportionment results. However, larger *a* values correspond to higher freedom of the solution space which led to potential mixing as the extreme case of *a* value of 1 which is equivalent to free PMF while extremely tight constraint (e.g., *a* value of 0) resulted in large residues (Lin et al., 2017). Therefore, the solution with an *a* value of 0.1 was chosen as the most appropriate one.

Figure S6 shows the mass spectra of HOA, COA, and OOA, as well as their diurnal patterns and relative contribution at *a* value of 0.1. The HOA profile was dominated by peaks at *m/z* of 27, 29, 41, 43, 55, and 57, characteristic of the hydrocarbon ion series of $[C_nH_{2n+1}]^+$ and $[C_nH_{2n-1}]^+$. The COA profile is characterized with a *f55* to *f57* ratio of 2.6 (where *f55* and *f57* are the fraction of *m/z* 55 and 57 to the total organic mass, respectively) which was higher than that for HOA (0.9) but was in the range of 2.2-2.8 typical found for COA (Mohr et al., 2012). The *f55* vs. *f57* plot (Fig. S9) provided further evidence that downtown Dublin was strongly affected by cooking activities as many OA points lied on the left-hand side of the triangular space defined by Mohr et al. (2012), consistent with the fact that there were many restaurants around the sampling site in downtown Dublin. The OOA profile featured a high *f44* value of 0.22 and did not contain significant contributions from marker peaks of other organic aerosol classes such as at *m/z* 55 or 60. The OOA profiles resemble more to the less volatile OOA (LV-OOA) which is often taken to represent well-aged SOA (Canonaco et al., 2013; Crippa et al., 2014). However, the diurnal pattern of OOA in Dublin showed a clear pattern that was strongly influenced by local sources and was most likely from fresh SOA instead of well-aged SOA.

OA factors at the kerbside during P2

The diurnal pattern of OA at the kerbside showed the evening OA peak was dominant during P2, suggesting large contributions from residential heating as discussed in Sect. 3.2. Consistently, free PMF found a fourth factor associated with biomass burning (i.e., BBOA) during P2, in addition to HOA, COA, and OOA (Fig. S10). The presence of BBOA factor was confirmed by the elevated *f60* (fraction of *m/z* 60 to total OA) of ~0.009 during the night (Fig. S11), as *f60* is usually taken as a marker for biomass burning especially for periods when *f60* is above background level of ~0.003 (Alfarra et al., 2007; Cubison et al., 2011).

Wood and peat are two types of biomass that were consumed by <5% of the households as the heating sources in Dublin (CSO, 2016), with the rest ~95% households using electricity and natural gas which, however, were not expected to emit POA. Moreover, the mass spectra of the emissions from wood and peat burning both contained *f60* as found in our previous combustion experiment (Lin et al., 2017). Free PMF failed to separate the peat factor from wood because they were co-emitted from residential heating, demonstrating temporal covariation which was hard for free PMF to resolve (Canonaco et al., 2013; Lin et al., 2017). To evaluate their contribution, ME-2 was utilized to constrain both peat and wood with a tight constraint (*a* value of 0.1). Note that the evening emissions were local and relatively fresh, and thus their mass spectral profiles were not expected to vary too much from the reference profiles retrieved from the combustion experiments (Lin et al., 2017). As for coal burning, no mass spectral marker was available but the reference coal profile demonstrated higher fraction at high *m/z*'s compared to HOA, peat, and wood (Lin et al., 2017). The five-factor solution from free PMF contained a factor profile with higher distributions at high *m/z*'s and its diurnal showed peaks in the evening, suggesting a coal factor. Similarly, an *a* value of 0.1 was applied for the coal factor.

The peat profile featured peaks at *m/z* of 27, 29, 41, 43, 55, and 57 (Fig. S12), which was similar to HOA. However, the differences in *f60* between the peat factor and HOA suggested different sources. *f60* in the peat profile was 0.016 which was higher than that for HOA (<0.003), confirming its biomass nature (Cubison et al., 2011). Note that peat is an accumulation of partially decayed plant material which is harvested as an important source of fuel in Ireland (Tuohy et al., 2009). The incomplete decay of vegetation resulted in an increase *f60* when burned. However, *f60* in peat profile was lower than wood (0.072) as wood is relatively fresh vegetation, containing a higher fraction of *m/z* 60-related material e.g., levoglucosan (Alfarra et al., 2007; Lin et al., 2017).

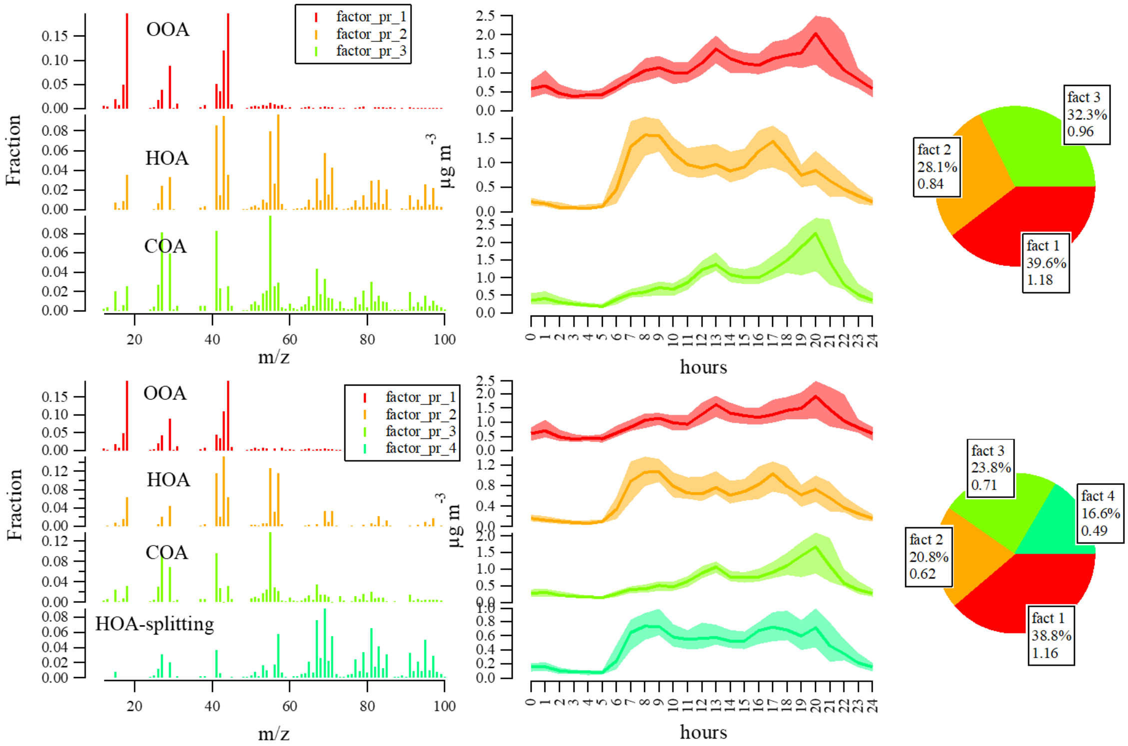

Figure S5. Mass spectral profiles (left panels) and diurnal (mid panels), as well as the relative contribution of the free PMF three- (top) and four- (bottom) factor solutions at the kerbside during P1. The four-factor solution shows a HOA splitting factor because its diurnal pattern was similar to HOA. For the diurnal cycles, the colored lines represent the median per hour of the day, and the shaded area the range between the 1st and the 3rd quartile of the data.

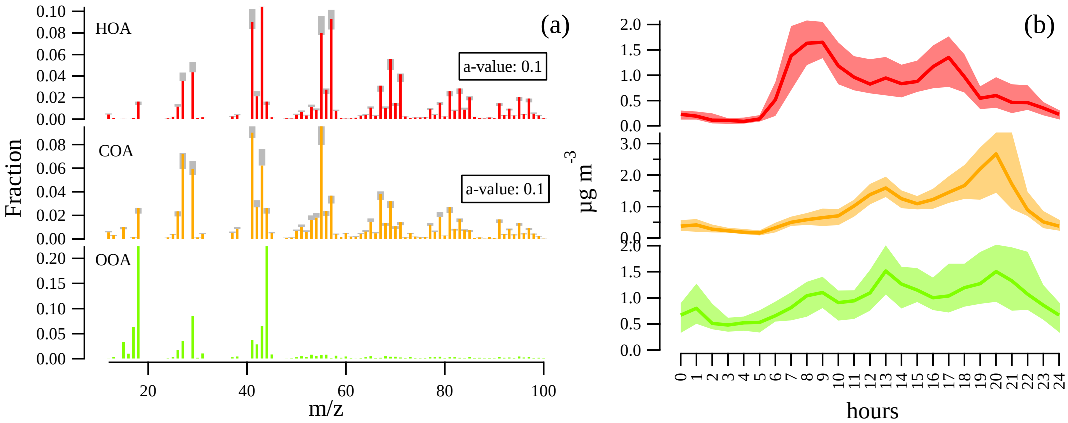

Figure S6. Mass spectra (a) and diurnal pattern (b) of HOA, COA, and OOA at the kerbside during P1. An *a* value of 0.1 was used to constrain the reference profiles of HOA and COA. The shaded area in (a) spans the area between lower and higher constrains with the center of the area representing the reference profile. For the diurnal cycles (b), the colored lines represent the median per hour of the day, and the shaded area the range between the 1st and the 3rd quartile of the data.

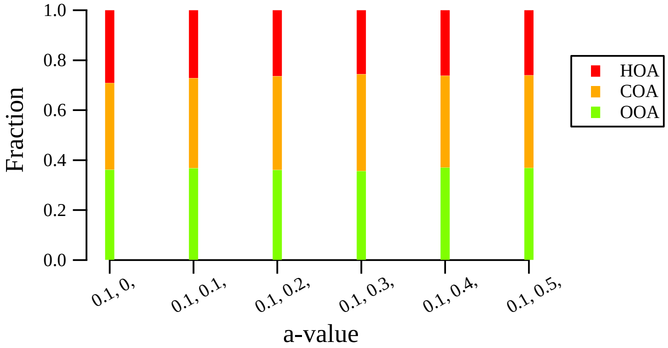

Figure S7. The relative contribution of HOA, COA, and OOA as a function of *a* value.

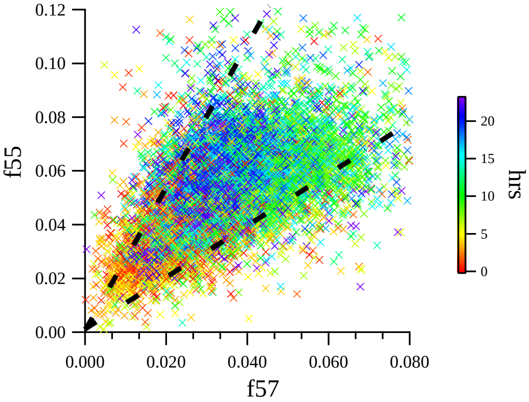

Figure S8. Triangular space of *f55* and *f57* color coded by hour of the day. The dash line was defined by Mohr et al. (2011).

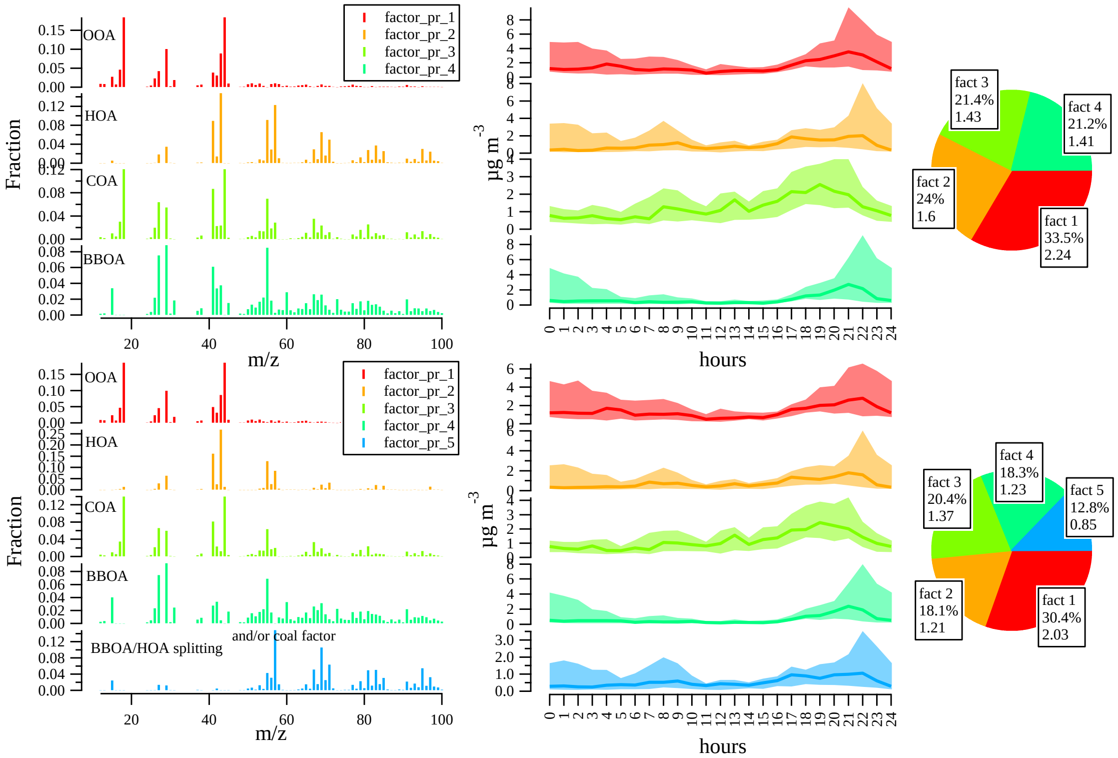

Figure S9. Mass spectral profiles (left panels) and diurnal (mid panels), as well as the relative contribution of the free PMF four- (top) and five- (bottom) factor solutions at the kerbside during P2. The four-factor solution shows a HOA splitting factor because its diurnal pattern was similar to HOA. For the diurnal cycles, the colored lines represent the median per hour of the day, and the shaded area the range between the 1st and the 3rd quartile of the data.

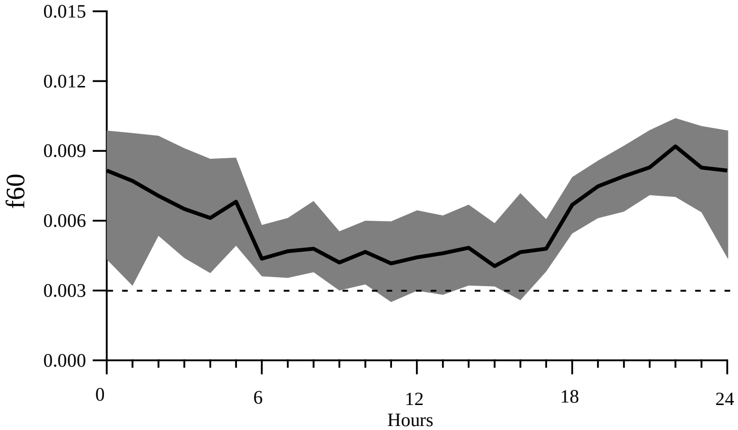

Figure S10. Diurnal pattern of f60 at the kerbside during P2. The colored lines represent the median per hour of the day, and the shaded area the range between the 1st and the 3rd quartile of the data. The dash line represents the background of f60 as found by Cubison et al. (2011).

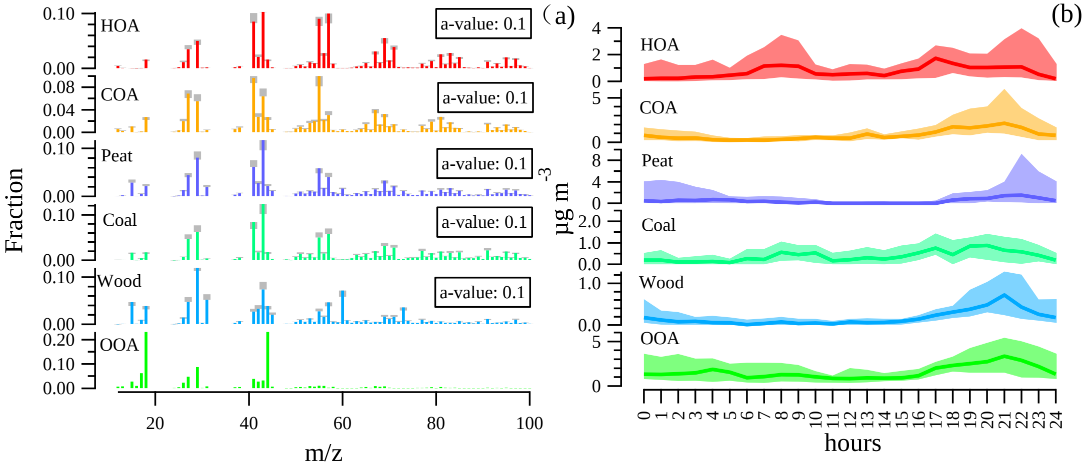

Figure S11. Mass spectra (a) and diurnal pattern (b) of HOA, COA, peat, coal, wood, and OOA at the kerbside during P2. An *a* value of 0.1 was used to constrain the reference profiles of HOA, COA, peat, coal, and wood. The shaded area in (a) spans the area between lower and higher constrains with the center of the area representing the reference profile. For the diurnal cycles (b), the colored lines represent the median per hour of the day, and the shaded area the range between the 1st and the 3rd quartile of the data.

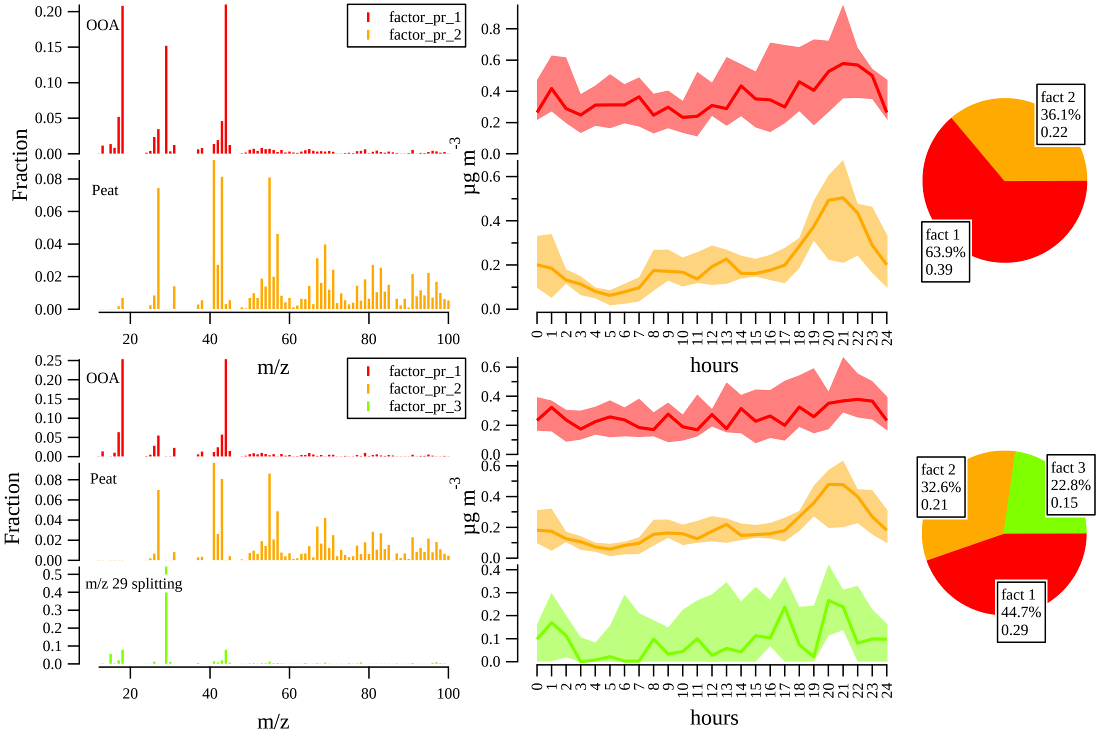

Figure 12. Mass spectral profiles (left panels) and diurnal (mid panels), as well as the relative contribution of the free PMF two- (top) and three- (bottom) factor solutions at the residential site during P1. The two-factor solution shows a m/z 29 splitting from other factors. For the diurnal cycles, the colored lines represent the median per hour of the day, and the shaded area the range between the 1st and the 3rd quartile of the data.

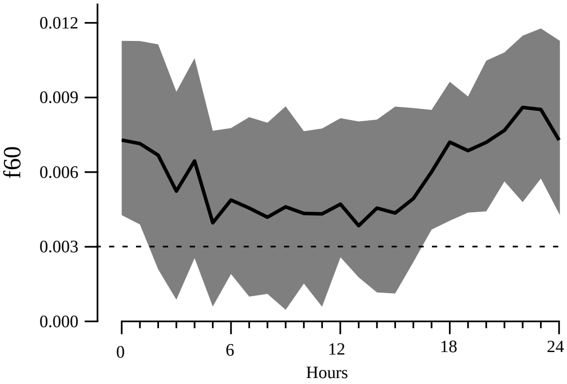

Figure S13. Diurnal pattern of *f60* at the residential site during P1. The colored lines represent the median per hour of the day, and the shaded area the range between the 1st and the 3rd quartile of the data. The dash line represents the background of *f60* as found by Cubison et al. (2011).

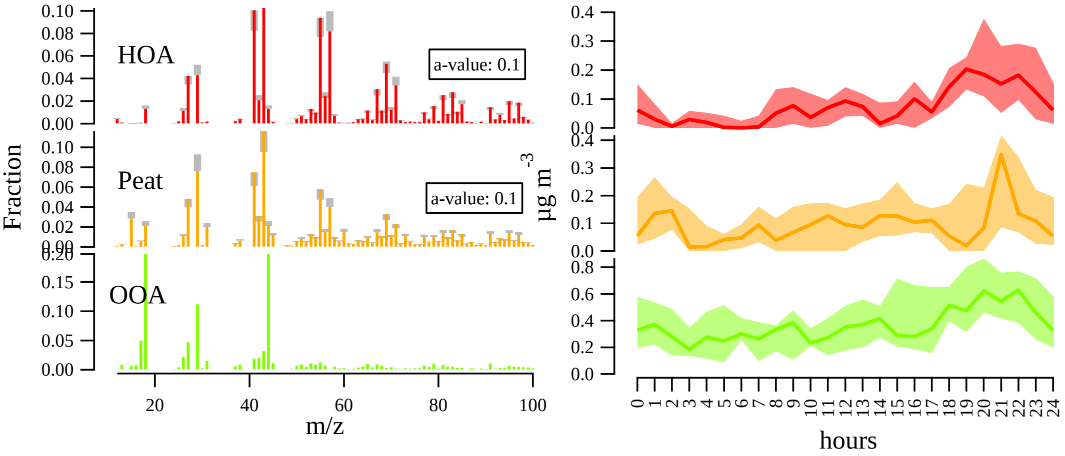

Figure S14. Mass spectra (left panel) and diurnal pattern (right panel) of HOA, peat, and OOA at the residential site during P1. An *a* value of 0.1 was used to constrain the reference profiles of HOA and peat. The shaded area in (a) spans the area between lower and higher constrains with the center of the area representing the reference profile. For the diurnal cycles (b), the colored lines represent the median per hour of the day, and the shaded area the range between the 1st and the 3rd quartile of the data.

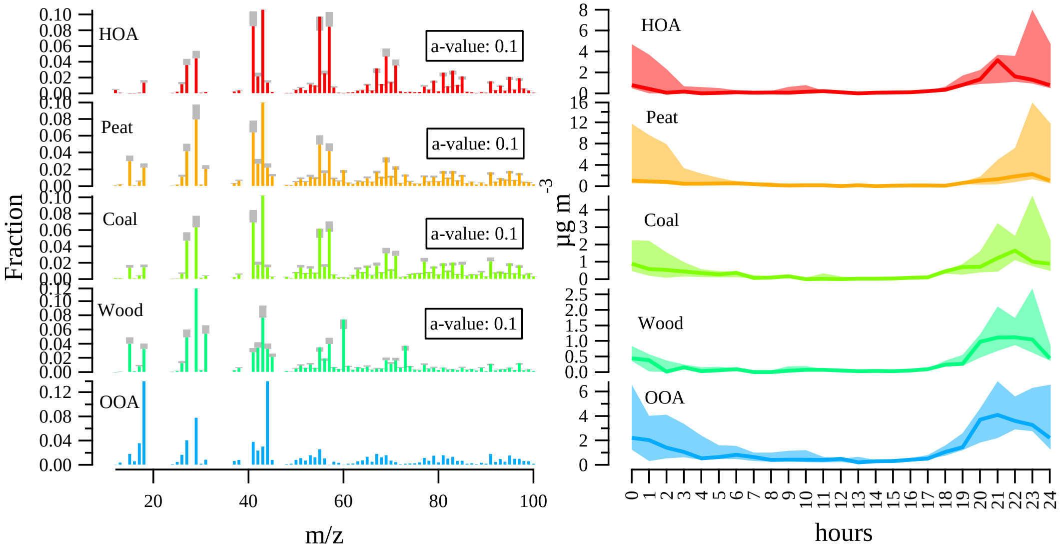

Figure S15. Mass spectra (left panel) and diurnal pattern (right panel) of HOA, peat, coal, wood, and OOA at the residential site during P2. An *a* value of 0.1 was used to constrain the reference profiles of HOA and peat. The shaded area in (a) spans the area between lower and higher constrains with the center of the area representing the reference profile. For the diurnal cycles (b), the colored lines represent the median per hour of the day, and the shaded area the range between the 1st and the 3rd quartile of the data.

Supplementary section of comparison between the kerbside and residential site

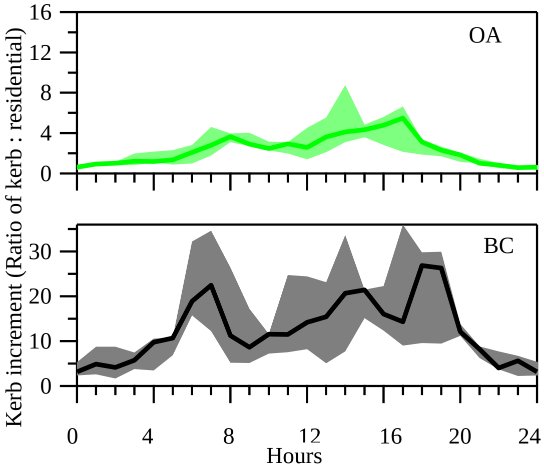

Figure S16. Diurnal cycles of the urban increment ratio for OA, BC, and NO$_x$. The colored lines represent the median per hour of the day, and the shaded area the range between the 1st and the 3rd quartile of the data

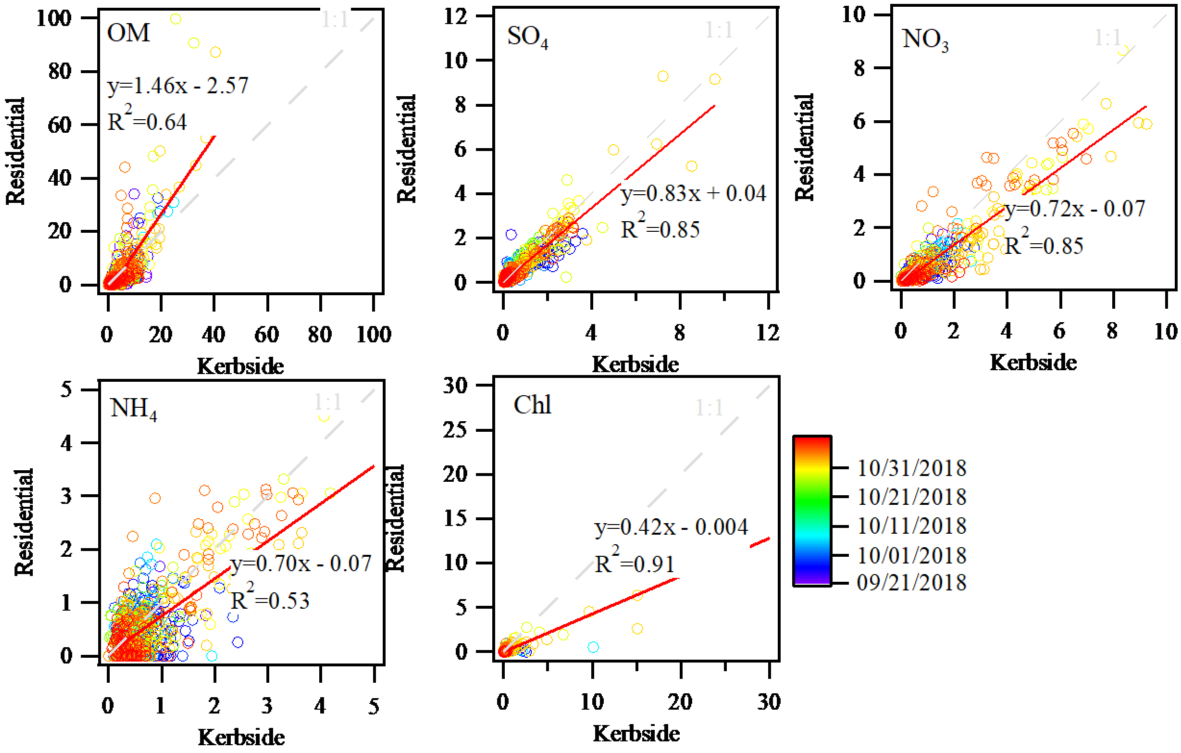

Figure S17. Linear regression for organic aerosol (OA), sulfate (SO$_4$), nitrate (NO$_3$), ammonium (NH$_4$), and chloride (Chl) between the kerbside (y-axis) and residential site (x-axis) over the entire campaign. All were hourly averaged and were in µg m^{-3}.

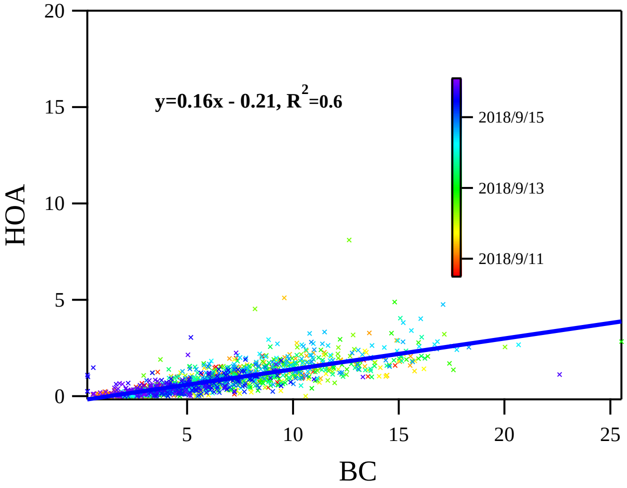

Figure S18. Linear regression between HOA and BC with a slope of 0.16 and R^2 of 0.6.

References:

Cubison, M. J., Ortega, A. M., Hayes, P. L., Farmer, D. K., Day, D., Lechner, M. J., Brune, W. H., Apel, E., Diskin, G. S., Fisher, J. A., Fuelberg, H. E., Hecobian, A., Knapp, D. J., Mikoviny, T., Riemer, D., Sachse, G. W., Sessions, W., Weber, R. J., Weinheimer, A. J., Wisthaler, A., and Jimenez, J. L.: Effects of aging on organic aerosol from open biomass burning smoke in aircraft and laboratory studies, Atmospheric Chemistry and Physics, 11, 12049-12064, 10.5194/acp-11-12049-2011, 2011.

Mohr, C., Richter, R., DeCarlo, P. F., Prévôt, A. S. H., and Baltensperger, U.: Spatial variation of chemical composition and sources of submicron aerosol in Zurich during wintertime using mobile aerosol mass spectrometer data, Atmospheric Chemistry and Physics, 11, 7465-7482, 10.5194/acp-11-7465-2011, 2011.